Cite as: Z. Ni *et al.*, *Science* 10.1126/science.abd8598 (2021).

Response to Comment on "Resolving spatial and energetic distributions of trap states in metal halide perovskite solar cells"

Zhenyi Ni, Shuang Xu, Jinsong Huang*

Department of Applied Physical Sciences, University of North Carolina, Chapel Hill, NC 27599, USA.

*Corresponding author. Email: jhuang@unc.edu

Ravishankar *et al.* claimed that drive-level capacitance profiling (DLCP) cannot resolve trap density in perovskites of given thickness. We point out that the trap densities derived by DLCP are from the differential capacitance at different frequencies; thus, the background charges caused by diffusion and geometry capacitance have been subtracted. Even for the nondifferential doping analysis, the contribution from diffusion capacitance is negligible and that from geometry capacitance is excluded.

In their Comment, Ravishankar *et al.* (*1*) derived an apparent carrier density distribution in semiconductor devices based on a capacitance model by assuming the combination of geometrical capacitance (C_g) and diffusion capacitance (C_d) as the dominant capacitance for semiconductor devices:

$$C = C_g + C_0 \exp\left(qV/mk_BT\right) \quad (1)$$

where q is elementary charge, V is the dc bias, m is the ideality factor [which was assumed to be 2 for the interpretation of Fig. 1C in (*1*)], k_B is the Boltzmann constant, and T is temperature. This is the equation upon which all their analysis is based. The authors derived the carrier density by assuming that this apparent (total) capacitance under forward bias follows the equations developed for reverse bias capacitance in a diode [eq. S8 in (*1*)], where the geometric and diffusion capacitance were not separated from the junction capacitance and were interpreted as part of the junction capacitance with the capacitance-voltage (CV) method. It is unknown whether this assumption stands, because neither geometrical nor diffusion capacitance is a function of carrier concentration. It is not appropriate to directly use the charge density from this CV method (small perturbation) to represent the carrier density from DLCP measurement (large perturbation), because studies have shown that the doping and charge densities were very likely to be skewed to larger values with the CV measurement if substantial densities of deep trap states exist within the depletion region (*2*). Even in (*3*), the experimental results showed that the CV measurement actually overestimated the free carrier density in the $CuInSe_2$ solar cell relative to the DLCP results by several times.

Nonetheless, even under the framework in which carrier density and profile distance directly from CV measurement are used to represent those from DLCP measurement, the following analysis shows that the geometry and diffusion capacitance have no impact on the measurement of charge trap densities by DLCP. Equation 1 predicts that carrier density is independent of applied ac frequency (ω); however, the experimental results in (*4*) showed a substantial frequency-dependent carrier distribution. The frequency-dependent capacitance is a critically important characteristic of charge traps and allows for the determination of their density with the DLCP method. Without a frequency-dependent carrier density, the traps would not show a trap-energy resolution as shown in figure 3 of (*4*). The trap density distributions shown in (*4*) were derived from the difference of the carrier densities at different ac frequencies under the same dc biases. The calculated carrier or trap density would be zero by the DLCP method if there is no frequency-dependent capacitance. In other words, the charge density derived from Eq. 1 does not show up as a background carrier density in the trap profiling derived from DLCP, and thus does not dismiss the application of DLCP in characterizing the trap densities.

Equation 1 does not represent the capacitance of a semiconductor device because it has a bias-independent constant junction capacitance of a p-n junction and also neglects the frequency dependence of C_d, although we understand that the trapping and detrapping of charge-

induced capacitance was omitted from this equation on purpose. The dependence of C_d on V and ac frequency ω of a typical n^+-p junction is reported in (*5*). As shown in the supplementary materials, this constraint means that Eq. 1 applies only at low ω. At high ω, the contribution of C_d to C reduces with a relationship of $C_d \propto \omega^{-0.5}$, which indicates that C_d is less important at higher ω. Therefore, the contribution of C_d to the measured doping (not trap) density is very small at high ω.

To verify whether C_d dominates C at large V in perovskite solar cells, we measured the C-V curves of a silicon diode (p-n junction) and perovskite single crystal and thin film solar cells at 62 kHz (Fig. 1A). The C-V of the silicon diode follows the relationship between C_d and V for $V \geq 0.4$ V (see supplementary materials), although the C-V response of the perovskite solar cell at large V did not follow Eq. 1. Because C_d is related to both V and ω (see supplementary materials), we further checked whether C was dominated by C_d at large V over a wide range of ω. The measured C-ω curves and the analytically calculated C_d-ω plots are shown in Fig. 1, B, C, and E. The parameters used for the calculation of the C_d-ω curves are summarized in table S1. Again, the calculated C_d-ω curves fit well for the Si diode in the low ac frequency region ($\omega\tau \ll 1$) where C_d is independent of ω (see supplementary materials), and C_d is proportional to $\omega^{-1/2}$ at high ac frequencies ($\omega\tau \gg 1$) (where τ is the minority carrier lifetime) (Fig. 1B).

In contrast, the calculated C_d values are 5 and 11 orders of magnitude smaller than the measured capacitance at large V over the wide range of ω for the thick single crystal and thin film perovskite solar cells, respectively (see supplementary materials). This difference is mainly attributed to the low minority carrier density in perovskites because of the self-doping of perovskite materials, which typically have a majority carrier density of ~10^{10} to 10^{15} cm^{-3} (*6*–*9*). Therefore, the C_d should be negligible in perovskite solar cells for V between 0 and 0.9 V adopted for the carrier density profiling in experiment. In this case, although the carrier densities calculated by the CV method have a U-shape similar to that measured by DLCP, it requires a substantially larger V of 1.0 to 1.6 V to complete the U-shape curve (fig. S1), which does not agree with the experimental data (0.2 to 0.9 V) in (*4*).

The measured C at different dc biases and frequencies in Fig. 1, C and E, also does not follow the response of C_d with ω predicted by eqs. S1 to S3. The measured C keeps increasing with the decrease of ω in the low ac frequency region, instead of being a constant. To understand the possible contributions from the charge transport layers to the frequency-dependent capacitance of the perovskite solar cells, as argued by Ravishankar *et al.*, we used the SCAPS software to simulate the C-ω curves of trap-free perovskite solar cells with both charge transport layers (*10*). As shown in Fig. 1, D and F, the trend of the simulated C-ω curves basically resembles the analytically calculated C_d-ω curves, both showing a constant C at ω below 10^5 Hz, distinctly different from the C-ω curves measured in experiment. We attribute this difference to the contribution of deep trap states from the junction capacitance. Moreover, even at the plateau region of the measured C-ω curves, C did not increase exponentially with V. These results further show that the measured C for perovskite solar cells at forward dc biases was still dominated by junction capacitance and charge trapping and detrapping capacitance, Any further analysis based on Eq. 1 would be inaccurate without taking the junction capacitance into consideration, especially when the doping and trap distributions are not uniform in the perovskite.

Finally, we may also use DLCP to evaluate doping density distribution in semiconductor devices by conducting the measurement at high frequency. An absence of subtraction process imposed the question of whether the measured carrier density is correct. We recently showed that the carrier density measured by DLCP in the perovskite films with thickness of 1 μm changed after aging, and had a lower carrier density (~3×10^{14} cm^{-3}) than that calculated by Ravishankar *et al.* (*11*), which indicates that C_d still did not dominate. Here we estimated the possible contribution of the C_d-caused "interfacial carrier density" to the DLCP measured carrier densities in perovskite solar cells by treating C_d in the same way as we did in DLCP measurement (see supplementary materials) (figs. S2 and S3). The contribution of C_d was clearly negligible because the of high frequency of measurement and small minority carrier density, indicating that the measured interfacial charge densities in perovskite solar cells were not caused by the charge injections. In addition, the influence of C_g on the carrier density measurement is prominent only when the applied bias is more than enough to fully deplete the perovskite layers, which was actually excluded in the carrier density profiling by DLCP measurement (see supplementary materials) (figs. S4 and S5).

REFERENCES

1. S. Ravishankar, T. Unold, T. Kirchartz, Comment on "Resolving spatial and energetic distributions of trap states in metal halide perovskite solar cells". *Science* **371**, eabd8014 (2021).
2. J. V. Li, G. Ferrari, *Capacitance Spectroscopy of Semiconductors* (Routledge, 2018), chapter 4.
3. J. T. Heath, J. D. Cohen, W. N. Shafarman, Bulk and Metastable Defects in $CuIn_{1-x}Ga_xSe_2$ Thin Films using Drive-Level Capacitance Profiling. *J. Appl. Phys.* **95**, 1000–1010 (2004). doi:10.1063/1.1633982
4. Z. Ni, C. Bao, Y. Liu, Q. Jiang, W.-Q. Wu, S. Chen, X. Dai, B. Chen, B. Hartweg, Z. Yu, Z. Holman, J. Huang, Resolving spatial and energetic distributions of trap states

in metal halide perovskite solar cells. *Science* **367**, 1352–1358 (2020). doi:10.1126/science.aba0893 Medline

5. S. M. Sze, K. K. Ng, *Physics of Semiconductor Devices* (Wiley, 2006), pp. 100–102.
6. D. Shi, V. Adinolfi, R. Comin, M. Yuan, E. Alarousu, A. Buin, Y. Chen, S. Hoogland, A. Rothenberger, K. Katsiev, Y. Losovyj, X. Zhang, P. A. Dowben, O. F. Mohammed, E. H. Sargent, O. M. Bakr, Low trap-state density and long carrier diffusion in organolead trihalide perovskite single crystals. *Science* **347**, 519–522 (2015). doi:10.1126/science.aaa2725 Medline
7. Y. Chen, H. T. Yi, X. Wu, R. Haroldson, Y. N. Gartstein, Y. I. Rodionov, K. S. Tikhonov, A. Zakhidov, X.-Y. Zhu, V. Podzorov, Extended carrier lifetimes and diffusion in hybrid perovskites revealed by Hall effect and photoconductivity measurements. *Nat. Commun.* **7**, 12253 (2016). doi:10.1038/ncomms12253 Medline
8. Q. Wang, Y. Shao, H. Xie, L. Lyu, X. Liu, Y. Gao, J. Huang, Qualifying composition dependent p and n self-doping in $CH_3NH_3PbI_3$. *Appl. Phys. Lett.* **105**, 163508 (2014). doi:10.1063/1.4899051
9. J. Peng, Y. Chen, K. Zheng, T. Pullerits, Z. Liang, Insights into charge carrier dynamics in organo-metal halide perovskites: From neat films to solar cells. *Chem. Soc. Rev.* **46**, 5714–5729 (2017). doi:10.1039/C6CS00942E Medline
10. M. Burgelman, P. Nollet, S. Degrave, Modelling polycrystalline semiconductor solar cells. *Thin Solid Films* **361–362**, 527–532 (2000). doi:10.1016/S0040-6090(99)00825-1
11. Y. Deng, Z. Ni, A. F. Palmstrom, J. Zhao, S. Xu, C. H. Van Brackle, X. Xiao, K. Zhu, J. Huang, Reduced Self-doping of Perovskites Induced by Short Annealing for Efficient Solar Modules. *Joule* **4**, 1949–1960 (2020). doi:10.1016/j.joule.2020.07.003

ACKNOWLEDGMENTS

Supported by Center for Hybrid Organic Inorganic Semiconductors for Energy (CHOISE), an Energy Frontier Research Center funded by the Office of Basic Energy Sciences, Office of Science within the U.S. Department of Energy. **Author contributions:** Z.N. and S.X. carried out the capacitance measurements, Z.N. performed the SCAPS simulations, J.H. and Z.N. wrote the paper, and all authors reviewed the paper. **Competing interests:** The authors declare that they have no competing interests. **Data and materials availability:** All data needed to evaluate the conclusions in the paper are present in the paper and in the references cited. Additional data related to this paper may be requested from the authors.

SUPPLEMENTARY MATERIALS

science.sciencemag.org/content/371/6532/eabd8598/suppl/DC1

6 August 2020; accepted 25 November 2020
Published online 26 February 2021
10.1126/science.abd8598

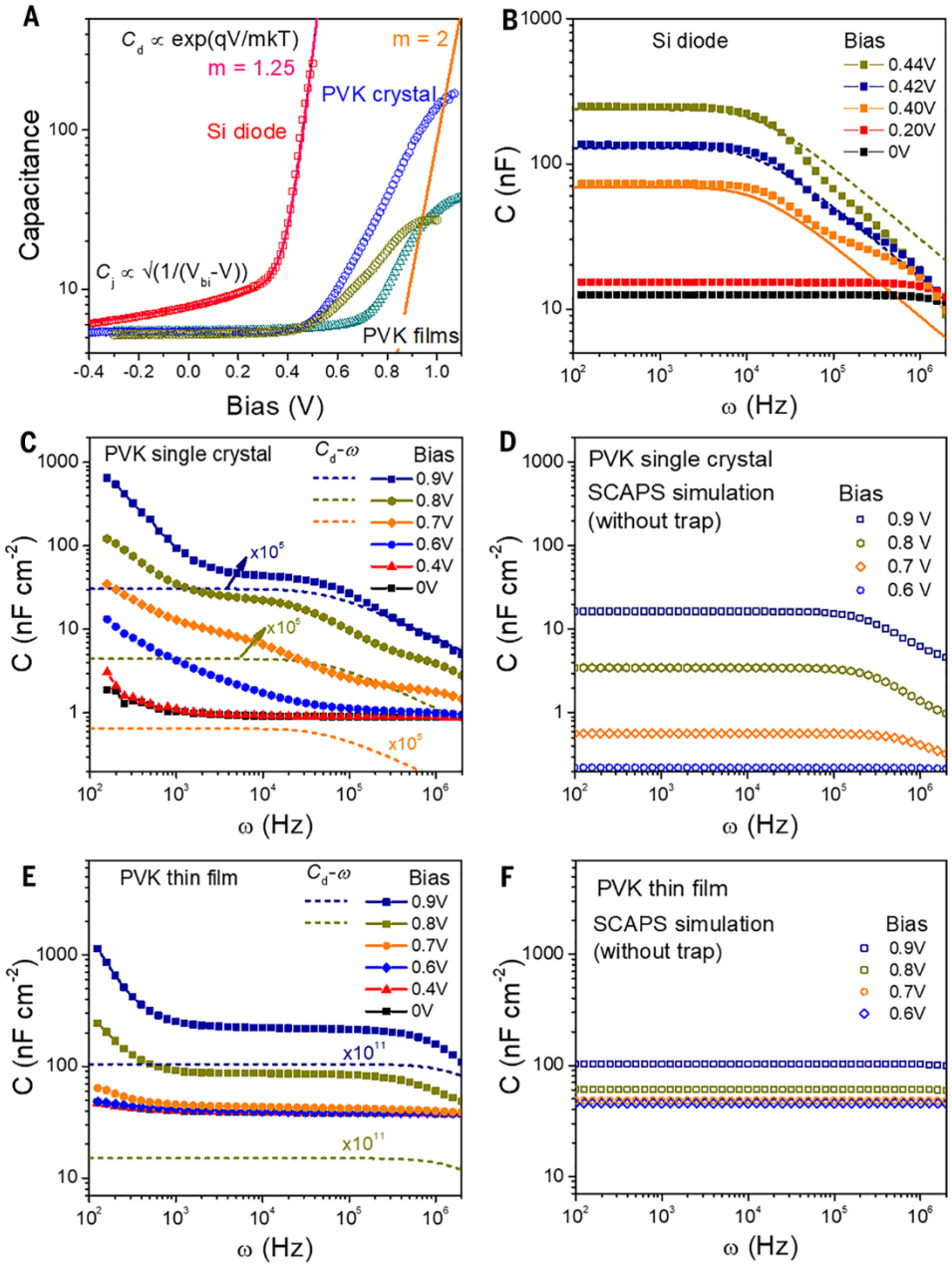

Fig. 1. Contribution of the diffusion capacitance to the total capacitances. (**A**) Normalized *C*-*V* curves of a Si diode (red), perovskite thin single crystal (PVK crystal) (blue), and polycrystalline thin film (PVK film) (green and khaki) solar cells measured at ac frequency (ω) of 62 kHz. The solid red and orange lines plot the dependence of C_d on $\exp(qV/mk_BT)$ with m = 1.25 and 2, respectively. (**B**, **C**, and **E**) *C*-ω curves of the Si diode (B), perovskite thin single crystal (C), and perovskite thin film solar cell (E) measured at difference dc biases. The dashed lines show the calculated C_d-ω curves with eq. S1 (see supplementary materials). (**D** and **F**) SCASP-simulated *C*-ω curves of a trap-free perovskite thin single crystal (D) and a perovskite thin film solar cell (F).

Response to Comment on "Resolving spatial and energetic distributions of trap states in metal halide perovskite solar cells"

Zhenyi Ni, Shuang Xu and Jinsong Huang

Science **371** (6532), eabd8598.
DOI: 10.1126/science.abd8598

science.sciencemag.org/content/371/6532/eabd8598/suppl/DC1

Supplementary Materials for

Response to Comment on "Resolving spatial and energetic distributions of trap states in metal halide perovskite solar cells"

Zhenyi Ni, Shuang Xu, Jinsong Huang*

*Corresponding author. Email: jhuang@unc.edu

Published 26 February 2021, *Science* **371**, eabd8598 (2021)
DOI: 10.1126/science.abd8598

This PDF file includes:

Table S1 Parameters used for the calculation of the diffusion capacitance.

Materials	N_C, N_V	E_g	n_i	n_{p0}	L_n	τ_n	m
Silicon		1.12 eV	1E10 cm^{-3}	2E5 cm^{-3}	450 μm	120 μs	1.25
Perovskite crystal	2E18 cm^{-3}	1.55 eV	1.8E5 cm^{-3}	3 cm^{-3}	10 μm	30 μs	2
Perovskite thin film	2E18 cm^{-3}	1.55 eV	1.8E5 cm^{-3}	3E-5 cm^{-3}	1 μm	1 μs	2

Discussion of the fitting parameters:

Effective density of states of conduction and valence bands (N_C, N_V): the effective density of states for the conduction and valence band of perovskite were chosen from the same reference used by Ravishankar *et al*.

Intrinsic carrier density (n_i): the n_i of silicon was chosen from (*1*). The n_i of perovskite is calculated by using $n_i = (N_C N_V)^{1/2} \exp(-E_g/2kT)$ at T = 300K. Though divergence may exist between the calculated and measured n_i, the difference of the values is basically within one order of magnitude for most semiconductors (*1*).

Minority carrier density (n_{p0}): for the silicon diode, the minority of the weakly doped side of the junction was calculated by $n_{p0} = n_i^2/p_{p0}$, where the majority carrier density p_{p0} was estimated from the Mott-Schottky plot of the silicon diode. For perovskite devices, the doping (majority carrier) density measured in $MAPbI_3$ single crystals was reported to be around 10^{10} cm^{-3} (*2*), and that measured in polycrystalline thin films was in the order of 10^{15} cm^{-3} (*3–5*). The n_{p0} in perovskite single crystal and thin films are calculated to be 3 cm^{-3} and 3×10^{-5} cm^{-3}, respectively.

Diffusion length of the minority (L_n): the L_n of silicon was read from (*6*). The L_n of thin perovskite single crystals was chosen from (*7*), which was around 10 μm. Most reported L_n of perovskite thin films were less than one micrometer (*8*). A representative value of 1 μm was chosen for the calculation of diffusion capacitances.

Minority carrier lifetime (τ_n): the minority carrier lifetime does not affect the calculation of the diffusion capacitance at low frequencies ($\omega\tau_n \ll 1$), but determines the demarcation frequency when the diffusion capacitance starts to drop with the further increase of ω. For silicon, the τ_n was chosen to be 120 μs which generates the best fitting results and also similar to the value listed in (*1*). For perovskite thin single crystal and thin films, τ_n were chosen to be close to the reported values in (*7*, *9*).

Diode ideality factor (m): the ideality factor was chosen in the range from 1 to 2. For the silicon diode, m = 1.25 was chosen to give the best fitting of the measured *C*-*V* plot. For perovskite devices, m = 2 was chosen to calculate the diffusion capacitances.

Table S2 Parameters used for the SCAPS simulations of the capacitance-frequency curves.

Parameter	PTAA	Perovskite	C_{60}
Thickness (nm)	10	39E3/500	25
Bandgap (eV)	3.30	1.55	1.90
Electron affinity (eV)	1.90	3.93	4.10
Dielectric permittivity (relative)	3	31	5
CB effective DOS (1/cm^3)	2E18	2E18	2E18
VB effective DOS (1/cm^3)	2E18	2E18	2E18
Electron thermal velocity (cm/s)	1E7	1E7	1E7
Hole thermal velocity (cm/s)	1E7	1E7	1E7
Electron mobility (cm²/Vs)	1E-3	10	1E-2
Hole mobility (cm²/Vs)	1E-3	10	1E-2
Shallow donor density ND (1/cm^3)	0	0	1E18
Shallow acceptor density NA (1/cm^3)	2E15	1E10/1E14	0
Radiative recombination coefficient (cm³/s)	0	1E-12	0

Supplementary Text

Dependence of diffusion capacitance on dc bias and ac frequency

The dependence of the diffusion capacitance (C_d) on the dc bias (V) and ac frequency (ω) of a typical n^+-p junction is derived from (*1*) by extending the dependence of the small-signal current density on voltage, for which the imaginary part gives the C_d:

$$C_d = \frac{Aq^2 n_{p0} L_n}{kT\tau_n} \exp\left(\frac{qV}{mkT}\right) \sqrt{\frac{\sqrt{1+\omega^2\tau_n^2}-1}{2\omega^2}}, \quad \text{(S1)}$$

where A is junction area, q is the elementary charge, n_{p0} is the minority (electron) carrier density of the p-type layer, L_n is the diffusion length of the minority in the p-type layer, k is the Boltzmann's constant, T is the temperature, τ_n is the minority carrier lifetime in the p-type layer, m is the ideality factor which ranges from 1 to 2 in all optimized perovskite solar cells.

At low frequencies ($\omega\tau_n \ll 1$), $\sqrt{1+\omega^2\tau_n^2} \approx 1 + \frac{\omega^2\tau_n^2}{2}$, C_d is approximated to

$$C_d = \frac{Aq^2 n_{p0} L_n}{2kT} \exp\left(\frac{qV}{mkT}\right), \quad \text{(S2)}$$

which is independent of frequency ω. At high frequencies ($\omega\tau_n \gg 1$), C_d is given by

$$C_d = \frac{Aq^2 n_{p0} L_n}{kT} \exp\left(\frac{qV}{mkT}\right) (2\omega\tau_n)^{-1/2}. \quad \text{(S3)}$$

As shown in Fig 1A, for the silicon diode, two regions with different bias ranges where the junction capacitance (C_j) and C_d dominant respectively can be clearly distinguished. The C_d-V

at the large bias region is well fitted by $C_d \propto \exp(qV/mkT)$ with m = 1.25. For perovskite solar cells, the *C*-*V* behaviors at large forward biases do not follow the characteristic of C_d on *V* with *m* up to 2, indicating C_d is not dominating the total capacitance even at high bias up to V_{OC}.

The C_d-ω curves of the silicon diode and perovskite solar cells are calculated by using equation (S1) with the parameters listed in Table S1. In the low frequency region, C_d is basically independent of ω, which is given by equation S2. In the high frequency region, C_d monotonously decreases with the increase of ω, following the relationship given by equation S3. For perovskite solar cells, the calculated C_d for perovskite single crystal and thin film solar cells at the low ac frequencies ($\omega\tau_n \ll 1$) and V = 0.9 V with the parameters listed in Table S1 are about 4×10^{-6} nF and 8×10^{-11} nF, respectively, which are at 5 and 11 orders of magnitude smaller than the measured C under the same conditions. Therefore, the influence of C_d on the total capacitance measured at large forward dc biases is negligible for perovskite solar cells.

Influence of the diffusion capacitance on the DLCP carrier doping density

Here we treated diffusion capacitance in the same way as what we did in DLCP measurement to find out how the diffusion capacitance impact the carrier doping concentration in DCLP measurement. In DLCP measurement, a series of changing ac biases (δV) are applied to the junction. The carrier density including doping and trap density is derived from the coefficients C_0 and C_1 from the dependence of the total C on δV:

$$C = C_0 + C_1\delta V + C_2\delta V^2 \ldots \quad \text{(S4)}$$

$$N_{DLCP} = -\frac{C_0^3}{2A^2 q\varepsilon_r\varepsilon_0 C_1} \quad \text{(S5)}$$

Now we discuss how C_d would affect C_0 and C_1 at larger forward dc biases during the DLCP measurement. In DLCP measurement, δV refers to the peak-to-peak value of the ac biases, and for each δV applied a compensatory dc bias of -1/2δV is added to the total bias to make the maximum applied forward voltage constant and fix the measurement region (*10*). If the C_d is not dependent on ac biases, as given by equation S1, the dependence of C_d on δV at a given forward dc bias of V_0 is

$$C_d = C'\exp\left(\frac{q\left(V_0-\frac{1}{2}\delta V\right)}{mkT}\right) \quad \text{(S6)}$$

$$= C'\exp\left(\frac{qV_0}{mkT}\right)\left[1-\frac{q}{2mkT}\delta V+\frac{q^2}{8m^2k^2T^2}\delta V^2 \ldots\right] \quad \text{(S7)}$$

where $C' = \frac{Aq^2 n_{p0}L_n}{2kT}$ or $\frac{Aq^2 n_{p0}L_n}{2kT}\left(\frac{2}{\omega\tau_n}\right)^{1/2}$ when $\omega\tau_n \ll 1$ or $\omega\tau_n \gg 1$, respectively.

Writing the C_d in the form of $C_d = C_{d0} + C_{d1}\delta V + C_{d2}\delta V^2$ ..., we can obtain:

$$C_{d0} = C'\,exp\left(\frac{qV_0}{mkT}\right), \quad \text{(S8)}$$

$$C_{d1} = -\frac{q}{2mkT}C'\,exp\left(\frac{qV_0}{mkT}\right). \quad \text{(S9)}$$

Comparing equations S8 and S9, we can obtain $\frac{C_{d1}}{C_{d0}} = -\frac{q}{2mkT} \approx -\frac{19.4}{m}$ (V^{-1}) at T = 300K.

For the Si diode measured at the dc bias of 0.4 V and ac frequency of 62 kHz, the numerical values of C_0 and C_1 derived from the polynomial fitting of C on δV are 9.02e-8 and -1.34e-6, respectively (Fig. S2A), which agrees with the relationship between C_{d0} and C_{d1} with m = 1.29, demonstrating a typical characteristic of the diffusion capacitance at this dc bias. The derived

m value is consistent with that obtained from the *C*-*V* and *C*-ω plots of the Si diode at low ac frequencies. At a high ac frequency of 1.8 MHz, the ratio of the numerical values of C_1/C_0 was around -2.2 at the dc bias of 0.4 V (Fig. S3A), which does not agree with the ratio of C_{d1}/C_{d0} with *m* up to 2. This indicates that C_d should no longer dominate the measured *C* at the high ac frequency regime for the Si diode, which is again reasonable. This analysis shows that the frequency dependent capacitance should not be ignored in calculating the total capacitance.

For perovskite single crystal and polycrystalline thin film solar cells, the derived C_1/C_0 ratios at the dc bias of 0.9 V and the ac frequency of 62 kHz are about -4.9 and -3.9, respectively (Figs. S2B, C), which significantly differ from the ratio of C_{d1}/C_{d0} with *m* up to 2 which is about -10. Here we have to consider the contribution of junction capacitance (C_j) to explain the significant different C_1/C_0 ratios at a large dc bias of 0.9 V:

$$C = C_j + C_d \tag{S10}$$

Then we have $C_0 = C_{j0} + C_{d0}$, $C_1 = C_{j1} + C_{d1}$. For $m = 2$, $C_{d1} = -10C_{d0}$. Since the measured $C_1/C_0 > -5$, substituting C_{d1} with $-10C_{d0}$ and combining $C_{j1} < 0$, we can have $C_0 > 2C_{d0}$. Writing $C_0 = 2C_{d0} + \Delta C$ where $\Delta C > 0$, the total (N_{tot}) and diffusion-induced (N_d) carrier densities can be estimated by:

$$N_{tot} = -\frac{C_0^3}{2A^2 q\varepsilon_r\varepsilon_0 C_1} > \frac{C_0^2}{10A^2 q\varepsilon_r\varepsilon_0} = \frac{(2C_{d0}+\Delta C)^2}{10A^2 q\varepsilon_r\varepsilon_0}, \tag{S11}$$

$$N_d = -\frac{C_{d0}^3}{2A^2 q\varepsilon_r\varepsilon_0 C_{d1}} = \frac{C_{d0}^2}{20A^2 q\varepsilon_r\varepsilon_0}. \tag{S12}$$

As a result, N_{tot} is at least 8 times larger than N_d for the perovskite solar cells at the dc bias of 0.9 V and at frequency of 62 kHz (corresponding the interface), even without considering the theoretical limitation of C' by using the parameters listed in Table S1. A quick way to check the possible maximum contribution of N_d to N_{tot} is by calculating $(-C_1/10C_0)^3$ at different forward dc biases. At the high ac frequency of 1.8 MHz, the derived C_1/C_0 ratios for the perovskite thin single crystal and polycrystalline thin film solar cells at the dc bias of 0.9 V were -3.8 and -2.7, respectively (Figs. S3B, C). As a result, the interfacial N_{tot} is at least 17 and 50 times larger than N_d for the perovskite single crystal and thin film solar cells respectively at the high ac frequency of 1.8 MHz (Figs. S4C, S5C). Once the actual C' in the real perovskite devices is adopted (see above), C_{d0} would be orders of magnitude smaller than C_{j0}, making the influence of the charge injections to the interfacial carrier/doping densities really negligible.

Influence of the geometrical capacitance on the DLCP carrier doping density

In DLCP measurement, the applied dc bias sweep the depletion region from one interface toward the other to scan the charge and trap distribution. There is a critical dc bias to fully deplete the perovskite layer. When the applied bias is larger than this critical value, $N(w) = -2(dC^{-2}/dV)^{-1}/q\varepsilon_r\varepsilon_0$ tells the actual doping concentration when there is no trapping based on the Schottky-Mott analysis. When the applied bias is smaller than this critical value, the capacitance does not change anymore, which equals to the geometrical capacitance C_g and thus dC^{-2}/dV is almost zero, which gives the huge carrier density in Ravishankar *et al*. We excluded the data for the biases less than the critical value, because when the depletion region reaches the metal/perovskite interface, there is no point to increase the reverse bias to further push the depletion region edge.

Since C_g is independent of dc biases, the coefficients of the high order terms of δV (C_1, C_2…) in equation S4 should be infinitely small or zero when the C_g dominates the total *C*. This would causes significant variation of C_0, and C_1 from the fitting of *C* on δV, thus leading to invalid

carrier densities calculated (Figs. S4, S5). In our measurement, we carefully excluded this situation to occur, ruling out the influence of the C_g on the measured carrier density distributions in perovskite solar cells. For the $MAPbI_3$ thin single crystal solar cells, dc biases below 0.20 V and above 0.95 V were excluded from the fitting. For the polycrystalline thin film solar cells, typically the dc bias below 0.55 V and above 0.95 V were excluded from the fitting.

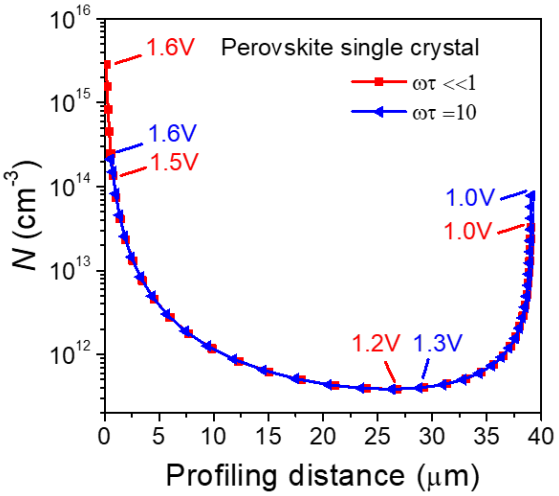

Fig. S1. CV method calculated carrier density distributions in a perovskite single crystal solar cell based on the assumption $C = C_g + C_0 \exp(qV/mkT)$ at low ac frequency ($\omega\tau \ll 1$) and high ac frequency ($\omega\tau = 10$). Here $C_g = 0.68$ nF/cm^2 (equals to the measured geometrical capacitance of a perovskite thin single crystal solar cell), C_0 is the pre-factor of the diffusion capacitance which was given by equation S1 of the technical response at different ac frequency ranges, and $m = 2$ was used for the calculations of the diffusion capacitance.The dc biases needed to achieve the corresponding carrier densities are denoted close to the curves. In experiment of (*11*), the adopted bias range for the DLCP carrier density profiling was 0.2 - 0.9 V, which is very different from the bias here.

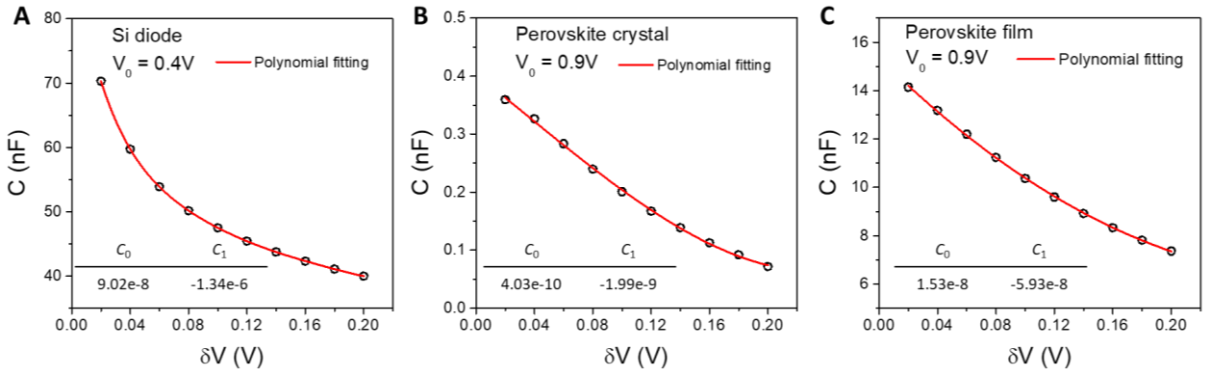

Fig. S2. Influence of the diffusion capacitance at large forward bias and low frequency. Dependence of the capacitance on the ac bias δV at a large forward dc bias (V_0) for the (A) silicon diode, (B) perovskite thin single crystal solar cell and (C) perovskite thin film solar cell measured at the ac frequency ω of 62 kHz. The numerical values of C_0 and C_1 derived from the polynomial fitting of C-δV with $C = C_0 + C_1\delta V + C_2\delta V^2$…are listed inside the figure.

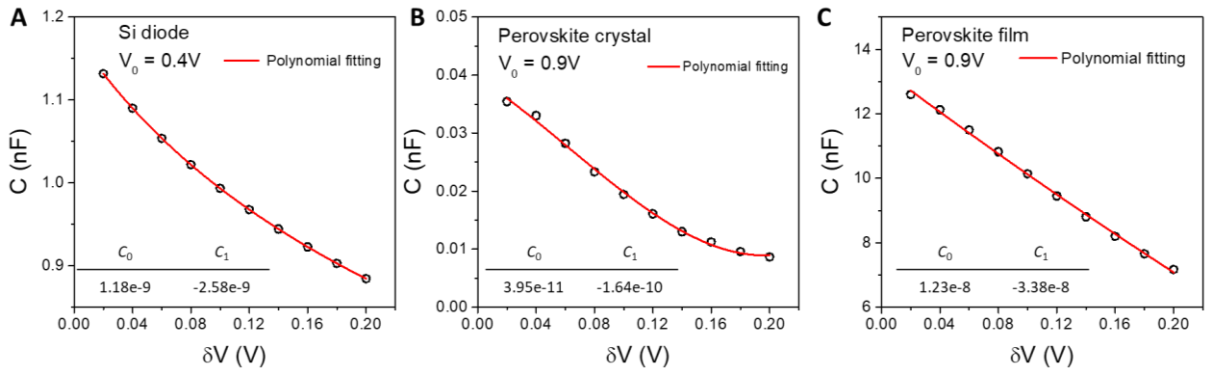

Fig. S3. Influence of the diffusion capacitance at large forward bias and high frequency. Dependence of the capacitance on the ac bias δV at a large forward dc bias (V_0) for the (A) silicon diode, (B) perovskite thin single crystal solar cell and (C) perovskite thin film solar cell measured at the ac frequency ω of 1.8 MHz. The numerical values of C_0 and C_1 derived from the polynomial fitting of C-δV with $C = C_0 + C_1\delta V + C_2\delta V^2$…are listed inside the figure.

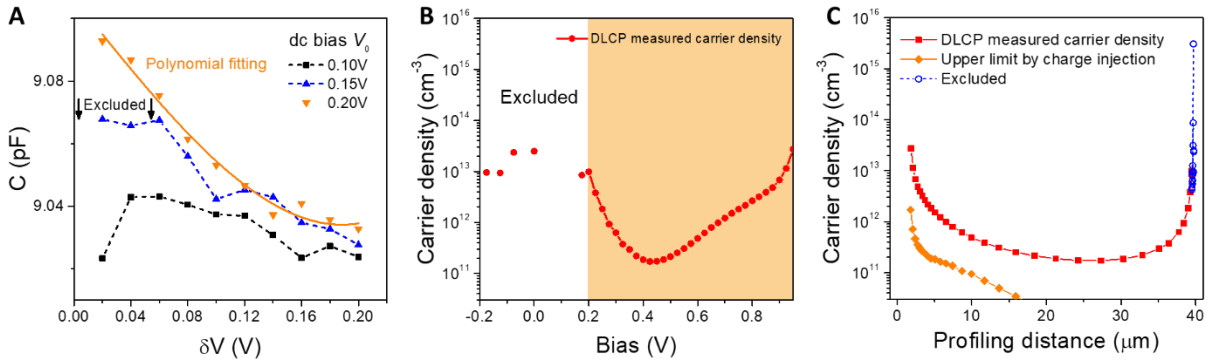

Fig. S4. DLCP measurement of a perovskite single crystal solar cell at high ac frequency. (A) Dependence of the capacitance on the ac bias δV at small forward dc biases (V_0) for a perovskite thin single crystal solar cell measured at the ac frequency ω of 1.8 MHz. When the bias is less than 0.2 V, the C - δV showed an irregular shape, resulting in invalid fitting for C_0 and C_1. (B) Dependence of the carrier densities on the dc bias measured by DLCP at ω of 1.8 MHz. (C) DLCP measured carrier density distribution in the perovskite single crystal solar cell at ω of 1.8 MHz. Those invalid data point measured at the dc biases smaller than 0.2 V are marked by blue circles. The upper limit carrier density by charge injections is derived from the analysis detailed above.

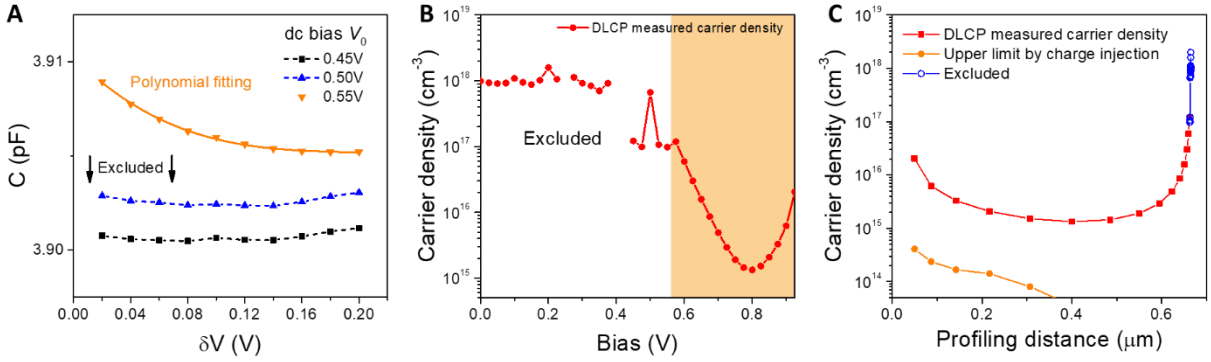

Fig. S5. DLCP measurement of a perovskite thin film solar cell at high ac frequency. (A) Dependence of the capacitance on the ac bias δV at small forward dc biases (V_0) for a perovskite thin film solar cell measured at the ac frequency ω of 1.8 MHz. When the bias is less than 0.55 V, the C - δV showed an irregular shape, resulting in invalid fitting for C_0 and C_1. (B) Dependence of the carrier densities on the dc bias measured by DLCP at ω of 1.8 MHz. (C) DLCP measured carrier density distribution in the perovskite thin film solar cell at ω of 1.8 MHz. Those invalid data point measured at the dc biases smaller than 0.5V are marked by blue circles. The upper limit carrier density by charge injections is derived from the analysis detailed above.

References

1. S. M. Sze, K. K. Ng, *Physics of Semiconductor Devices* (Wiley, 2006), pp. 100–102.

2. D. Shi, V. Adinolfi, R. Comin, M. Yuan, E. Alarousu, A. Buin, Y. Chen, S. Hoogland, A. Rothenberger, K. Katsiev, Y. Losovyj, X. Zhang, P. A. Dowben, O. F. Mohammed, E. H. Sargent, O. M. Bakr, Low trap-state density and long carrier diffusion in organolead trihalide perovskite single crystals. *Science* **347**, 519–522 (2015). doi:10.1126/science.aaa2725 Medline

3. Y. Chen, H. T. Yi, X. Wu, R. Haroldson, Y. N. Gartstein, Y. I. Rodionov, K. S. Tikhonov, A. Zakhidov, X.-Y. Zhu, V. Podzorov, Extended carrier lifetimes and diffusion in hybrid perovskites revealed by Hall effect and photoconductivity measurements. *Nat. Commun.* **7**, 12253 (2016). doi:10.1038/ncomms12253 Medline

4. Q. Wang, Y. Shao, H. Xie, L. Lyu, X. Liu, Y. Gao, J. Huang, Qualifying composition dependent p and n self-doping in $CH_3NH_3PbI_3$. *Appl. Phys. Lett.* **105**, 163508 (2014). doi:10.1063/1.4899051

5. J. Peng, Y. Chen, K. Zheng, T. Pullerits, Z. Liang, Insights into charge carrier dynamics in organo-metal halide perovskites: From neat films to solar cells. *Chem. Soc. Rev.* **46**, 5714–5729 (2017). doi:10.1039/C6CS00942E Medline

6. M. S. Tyagi, R. Van Overstraeten, Minority carrier recombination in heavily-doped silicon. *Solid-State Electron.* **26**, 577–598 (1983). doi:10.1016/0038-1101(83)90174-0

7. Z. Chen, Q. Dong, Y. Liu, C. Bao, Y. Fang, Y. Lin, S. Tang, Q. Wang, X. Xiao, Y. Bai, Y. Deng, J. Huang, Thin single crystal perovskite solar cells to harvest below-bandgap light absorption. *Nat. Commun.* **8**, 1890 (2017). doi:10.1038/s41467-017-02039-5 Medline

8. S. D. Stranks, G. E. Eperon, G. Grancini, C. Menelaou, M. J. P. Alcocer, T. Leijtens, L. M. Herz, A. Petrozza, H. J. Snaith, Electron-hole diffusion lengths exceeding 1 micrometer in an organometal trihalide perovskite absorber. *Science* **342**, 341–344 (2013). doi:10.1126/science.1243982 Medline

9. W. Q. Wu, Z. Yang, P. N. Rudd, Y. Shao, X. Dai, H. Wei, J. Zhao, Y. Fang, Q. Wang, Y. Liu, Y. Deng, X. Xiao, Y. Feng, J. Huang, Bilateral alkylamine for suppressing charge recombination and improving stability in blade-coated perovskite solar cells. *Sci. Adv.* **5**, eaav8925 (2019). doi:10.1126/sciadv.aav8925 Medline

10. J. T. Heath, J. D. Cohen, W. N. Shafarman, Bulk and Metastable Defects in $CuIn_{1-x}Ga_xSe_2$ Thin Films using Drive-Level Capacitance Profiling. *J. Appl. Phys.* **95**, 1000–1010 (2004). doi:10.1063/1.1633982

11. Z. Ni, C. Bao, Y. Liu, Q. Jiang, W.-Q. Wu, S. Chen, X. Dai, B. Chen, B. Hartweg, Z. Yu, Z. Holman, J. Huang, Resolving spatial and energetic distributions of trap states in metal halide perovskite solar cells. *Science* **367**, 1352–1358 (2020). doi:10.1126/science.aba0893 Medline